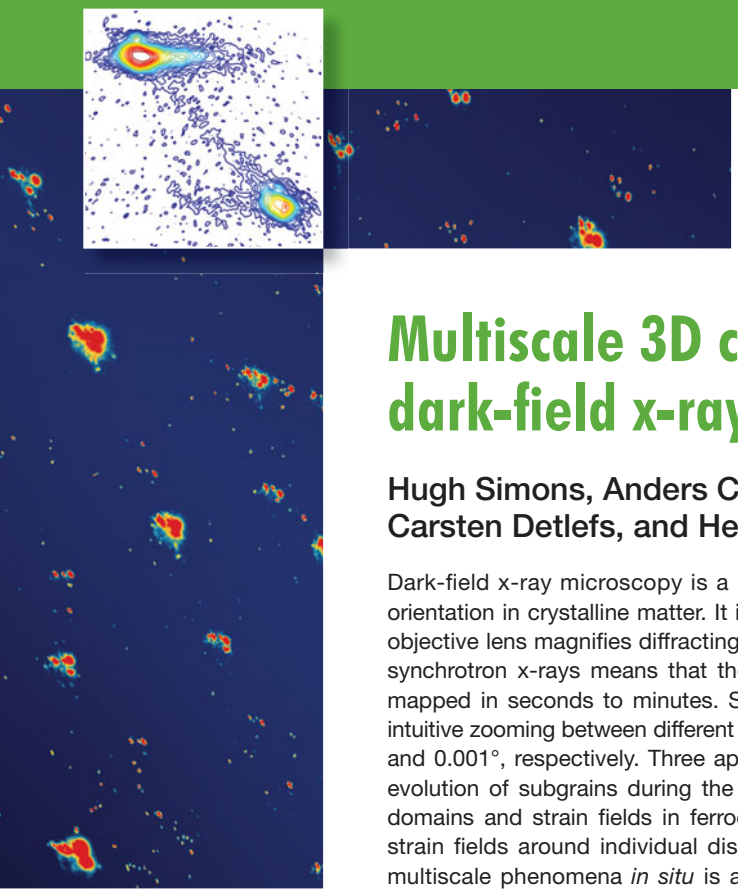


Multiscale 3D characterization with dark-field x-ray microscopy

Hugh Simons, Anders Clemen Jakobsen, Sonja Rosenlund Ahl, Carsten Detlefs, and Henning Friis Poulsen

Dark-field x-ray microscopy is a new way to three-dimensionally map lattice strain and orientation in crystalline matter. It is analogous to dark-field electron microscopy in that an objective lens magnifies diffracting features of the sample; however, the use of high-energy synchrotron x-rays means that these features can be large, deeply embedded, and fully mapped in seconds to minutes. Simple reconfiguration of the x-ray objective lens allows intuitive zooming between different scales down to a spatial and angular resolution of 100 nm and 0.001°, respectively. Three applications of the technique are presented—mapping the evolution of subgrains during the processing of plastically deformed aluminum, mapping domains and strain fields in ferroelectric crystals, and the three-dimensional mapping of strain fields around individual dislocations. This ability to directly characterize complex, multiscale phenomena *in situ* is a key step toward formulating and validating multiscale models that account for the entire heterogeneity of materials.

Introduction

Most materials and minerals are composed of hierarchical crystalline structures and substructures, such as grains, domains, and atomic-scale defect networks. A critical and persistent issue across materials and geological sciences is to understand and model the interplay of physical phenomena and structural dynamics at and between these different length scales. With this capability, the final macroscopic properties of a material can then be predicted from the initial microstructure and processing conditions, and materials can be designed and optimized using computer simulations rather than experimental trial and error. To guide such efforts, it is vital to develop experimental techniques that can rapidly swap between different length scales and make *in situ*, three-dimensional (3D) movies of the local changes to the crystalline lattice—structure, strain, and orientation.

The need to probe the local crystallography favors the use of diffraction-based approaches, yet existing 3D techniques have shortcomings with respect to multiscale characterization. Electron-based methods provide high spatial resolution, but are inherently destructive, as they are either limited to thin foils[1,2] or involve serial sectioning.[3,4] Scanning[5–10] and coherent[10–12] x-ray methods are rapidly progressing toward 20-nm resolution, but are limited to small sampling volumes. Furthermore, all methods face the challenge that the illuminated part of a bulk sample may comprise millions or even billions of structural elements whose diffracted signals overlap, preventing data analysis and interpretation.

Here, we describe dark-field x-ray microscopy, a new full-field imaging technique for nondestructively mapping structure, orientation, and strain of deeply embedded crystalline elements (e.g., within millimeter-sized samples) in 3D. By placing an x-ray objective lens in the diffracted beam, users can intuitively zoom between different length scales by changing the objective focal length, overcoming the spatial bandwidth limitations of other techniques. The objective also filters stray diffraction signals, suppressing unwanted overlap and isolating the individual structural element of interest.

This technique is readily combined with coarse-scale 3D grain-mapping techniques, such as 3D x-ray diffraction (3DXRD)[13–16] and diffraction contrast tomography (DCT),[17,18] as well as classical tomography. This combination enables the user to rapidly progress from fast overviews of an entire specimen to detailed studies of local phenomena in a single experimental setting.

Hugh Simons, Department of Physics, Technical University of Denmark, Denmark; husimo@fysik.dtu.dk
Anders Clemen Jakobsen, Department of Physics, Technical University of Denmark, Denmark; andcj@fysik.dtu.dk
Sonja Rosenlund Ahl, Department of Physics, Technical University of Denmark, Denmark; sroh@fysik.dtu.dk
Carsten Detlefs, European Synchrotron Radiation Facility, France; detlefs@esrf.fr
Henning Friis Poulsen, Department of Physics, Technical University of Denmark, Denmark; hfpo@fysik.dtu.dk
doi:10.1557/mrs.2016.114

© 2016 Materials Research Society
https://doi.org/10.1557/mrs.2016.114 Published online by Cambridge University Press

We demonstrate the applicability of the technique to three problems of interest in materials science—the processing of plastically deformed metals, the distribution of strain and orientation gradients in ferroelectrics, and the 3D morphology of dislocations.

Description of dark-field x-ray microscopy

The geometry and operational principle of dark-field x-ray microscopy (**Figure 1**) are conceptually similar to that of dark-field transmission electron microscopy (TEM). The diffracted beam passes through an x-ray objective lens, creating a magnified image of a specific region of interest with contrast from local variations in lattice symmetry, orientation, and strain. The sample-to-detector distance is typically 2–6 m, enabling magnification ratios of up to 50 while still maintaining sufficient space around the sample for *in situ* apparatus. Like the electron microscope, the x-ray microscope can be operated in a variety of modes. Maps of axial strain can be obtained by scanning the objective and detector through the scattering angle 2θ, while the local misorientation can be similarly mapped by scanning the sample through two orthogonal tilt directions (α, β).

Three-dimensional measurements of axial strain and orientation can be obtained in two ways: First, by using a one-dimensionally focusing condenser to create a narrow line beam[19] that illuminates a "slice" of the material (typically 200 µm × 200 µm × 200 nm), which is then imaged at an oblique angle. A 3D volume is then obtained layer wise by translating the sample through the planar beam in small increments. A second, faster method involves illuminating the entire grain and recording projections from different viewing angles while rotating the sample around the scattering vector, **Q**.[20] Three-dimensional reconstruction can then be accomplished using adapted tomographic algorithms.

A defining feature of the dark-field x-ray microscope is the x-ray objective. Like a visible light microscope, the x-ray objective can be reconfigured to adjust the magnification and numerical aperture, and hence the spatial resolution according to specific experimental requirements. Compound refractive x-ray lenses are typically used,[21] however, such optics are chromatic and have a significantly smaller numerical aperture than their visible light counterparts. The implications of this are threefold. First, the angular resolution is on the order of 0.001° to 0.03°, and thus, superior to those of electron microscopes. Second, the objective filters out diffraction signals from other unwanted regions of the sample, potentially allowing the study of a specific element out of 10^{10} or more within the illuminated volume. Third, the narrow angular acceptance necessitates prior knowledge of orientation of the region of interest. Such information is readily obtained from fast prescanning techniques, such as 3DXRD or DCT.

The studies described herein were performed *ad hoc* at beamline ID06 at the European Synchrotron Radiation Source (Grenoble, France), operating in the x-ray energy range of 15–30 keV. The current spatial resolution is ~100 nm, while the mapping of strain can, in favorable cases, be performed with a resolution of 10^{-5}. A dedicated x-ray microscope incorporating the dark-field modality is anticipated to be commissioned at this beamline in 2016 with a target resolution of 50 nm.

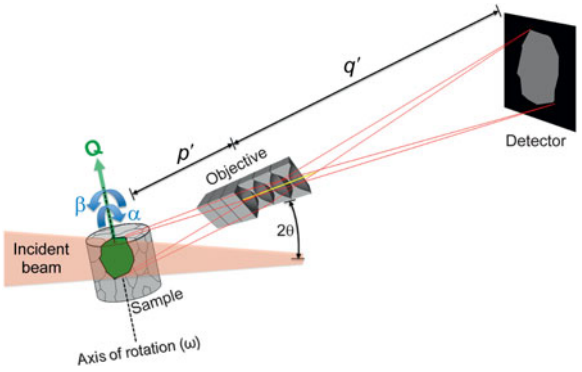


Figure 1. Principle of dark-field x-ray microscopy. Monochromatic x-rays illuminate a crystalline element of interest, and the diffracted radiation is imaged by means of an x-ray objective and a 2D detector. The magnification is approximately given by the ratio q'/p'. Scanning the sample tilt (α, β) and 2θ angles facilitates mapping of orientation and strain, respectively, while different projection angles can be obtained by rotating the sample around its scattering vector, **Q**.[22]

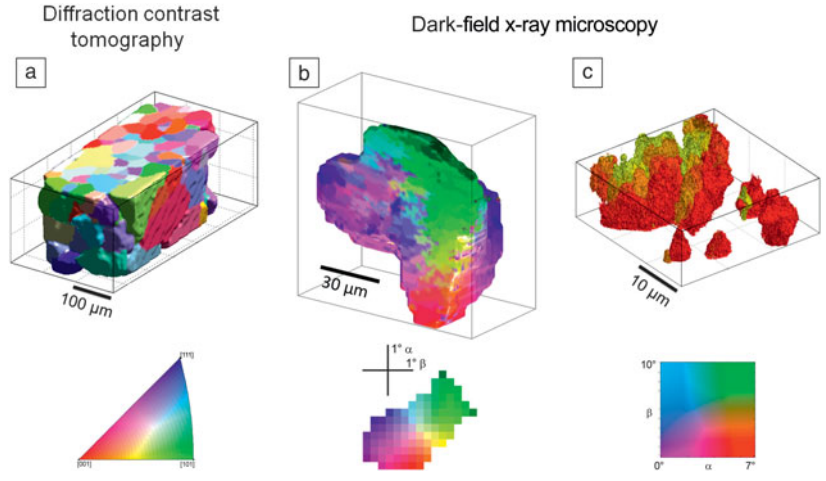


Figure 2. Multiscale mapping of 10% tensile deformed 1050 (99.5% pure) aluminum. (a) Part of a map of all grains in the specimen. (b) Zooming in on one grain and mapping the intrinsic variation in orientation. A vertical section through the grain is shown. (c) Additional zoom and mapping of selected individual subgrains in 3D. The spatial resolution from left to right is 3.5 µm, 1.5 µm, and 300 nm, and the angular resolution is 0.5°, 0.15°, and 0.03°, respectively. The colors symbolize orientations.[22]

https://doi.org/10.1557/mrs.2016.114 Published online by Cambridge University Press

Processing of plastically deformed metals

During plastic deformation, dislocations proliferate and self-organize to create hierarchical structures comprising grains, cell blocks, and individual subgrains surrounded by dislocation walls. At present, bottom-up modeling approaches are not capable of creating the complex structures observed using TEM. Furthermore, as heterogeneous events such as the nucleation of new grains or cracks tend to govern the structural evolution, state-of-the art models, at best, systematize generic features of the static structure. Hence fundamental questions remain regarding both the deformation process itself, and the nucleation and growth processes during subsequent annealing.

Figure 2 demonstrates how DCT and dark-field x-ray microscopy can be combined into a unique tool for 3D mapping structures at various length scales in deformed metals. For this study[22] of a needle-shaped Al sample with dimensions of 0.3 mm × 0.6 mm × 8 mm, an x-ray energy of 17 keV was used with image exposure times on the order of one second. Dark-field x-ray microscopy has the potential to directly visualize the formation and dissolution of subgrains, and their interactions with one another and their parent grains.

The high-angular resolution of dark-field x-ray microscopy also provides a way to detect fine-scale structures, such as lines of dislocations with low densities. As an example, **Figure 3** shows the substructure of a recrystallized Al grain with an angular difference across the observed internal boundaries of the order of 0.05°, corresponding to dislocations separated by more than 0.46 μm.[23] The intrusions in the external grain boundary seem to be related to the internal boundaries. Furthermore, unlike conventional techniques such as electron backscatter diffraction, dark-field x-ray microscopy provides a measure of the angular distribution associated with each voxel in the sample (Figure 3c). This is seen as a potential vehicle for improved estimations of local dislocation densities.

Relatively fast measurements of the dynamics can be conducted by assessing the collective statistics from individual subgrains, such as volume, average orientation, or average strain. During nucleation and growth processes, the evolution of such parameters can be monitored within hundreds or thousands of elements. As an example, **Figure 4** shows the subgrain size distribution in an Al sample after deformation at room temperature.[24] As anticipated, the distribution shifts toward larger and fewer grains upon heating.

Strain and domain mapping in ferroelectrics

A defining feature of ferroelectric materials is the presence of domains—regions of parallel spontaneous polarization that self-organize across several length scales to minimize the global free energy.[25] Under external fields, these domains can nucleate, grow, shrink, and annihilate through the collective motion of domain walls, facilitating a diverse range of applications, including memory, microelectromechanical systems, and ultrasound technology. Despite the crystallographic twinning relationship between neighboring domains, ferroelectrics tend to be distorted in the local vicinity of the domain wall, giving rise to complex local phenomena, such as conductivity[26] and polarization rotation.[27]

Understanding the relationship between domain topology, orientation, and stress around domain walls would therefore be a significant advance. Yet, the topologies and dynamics of ferroelectric domains are extremely complex—3D and

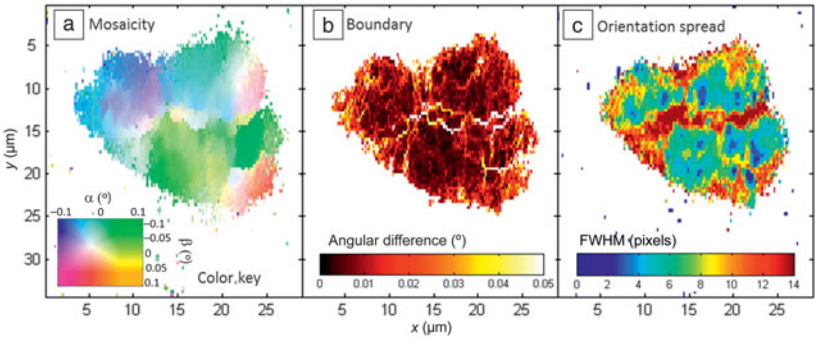


Figure 3. Structure of one layer of a recrystallized grain within a ~500-μm-sized 1050 (99.5% pure) aluminum sample. The distribution of angular spread of the (200) reflection is recorded for each voxel in terms of sample tilt (α, β) (as per Figure 1). (a) Map of the most intense angular setting for each voxel, (b) corresponding map of local misorientations, and (c) map of the full width at half maximum (FWHM) of the mosaic distribution for each voxel.[23]

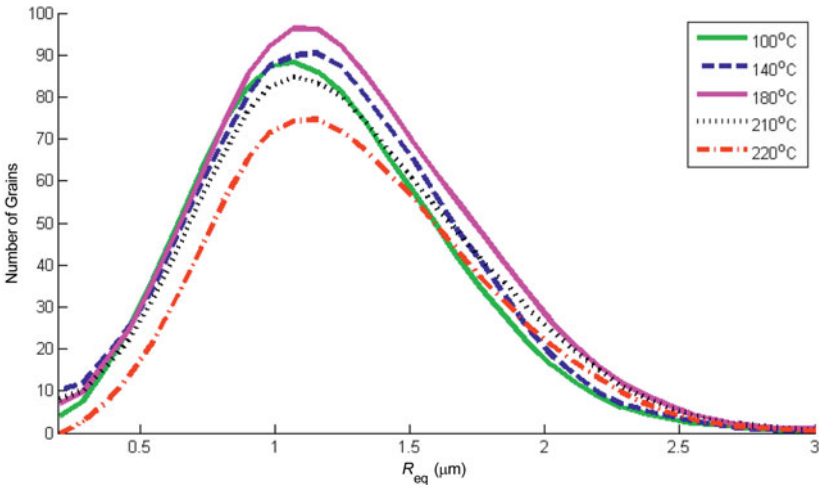


Figure 4. Histograms of subgrain size (defined as the equivalent spherical radius, R_{eq}) as a function of a linear increase in temperature during recovery of 1050 (99.5% pure) aluminum. The distribution is prone to experimental error below a radius of 1 μm.[24]

https://doi.org/10.1557/mrs.2016.114 Published online by Cambridge University Press

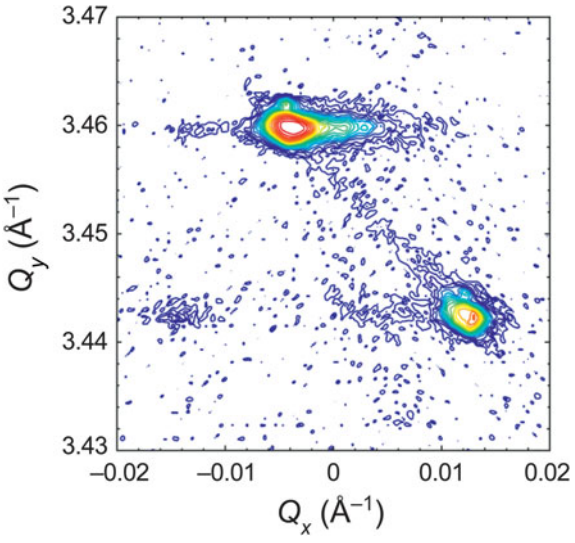


Figure 5. Reciprocal space map around the 220 reflection of a $KNbO_3$ ferroelectric crystal obtained as a rapid prescanning technique. The peaks correspond to the lattice spacing and orientation of domain variants. Q_x and Q_y are the reciprocal space directions corresponding to α and β. The contours correspond to a normalized log axis, where red is the highest intensity value.[28]

multiscale—and highly sensitive to internal and external boundary conditions. With dark-field x-ray microscopy, we can directly map the local variations in strain and orientation that occur at domain walls and other critical interfaces. In this example study,[28] the domain topology and strain distribution were mapped within an isolated region of an orthorhombic $KNbO_3$ ferroelectric crystal. The microscope imaged the 220 family of reflections at an x-ray energy of 17 keV to give a spatial resolution of 95 nm × 250 nm × 250 nm.

Figure 5 shows a coarse, nonspatially resolved overview of the orientation and strain distributions within the grain obtained by recording the far-field diffraction intensity distribution of the 220 family of reflections (i.e., without the objective in place).[28] The two intense peaks correspond to two domain variants dominating the sampling volume, however, it is their local structure and the intensity between them that is of interest. The peaks are not ideally Gaussian as expected, rather they are elongated and asymmetric with "wings" of intensity between them. These features are deviations from the presumed orthorhombic crystal symmetry of $KNbO_3$, and strongly indicate the presence of strain and orientation inhomogeneities associated with the domain topology.

The topological origin of this intensity distribution can be directly imaged using dark-field x-ray microscopy, as shown in **Figure 6**.[28] Both the orientation and strain maps show a topology consistent with contemporary microscopy techniques, containing stripe-shaped domains separated by non-180° ferroelastic domain walls. In particular, the strain map indicates clearly that strain gradients are a pervasive and significant feature in ferroelectric crystals. Zooming in both spatial and angular domains indicates that significant strain and lattice orientation gradients extend up to 2 μm into the material.

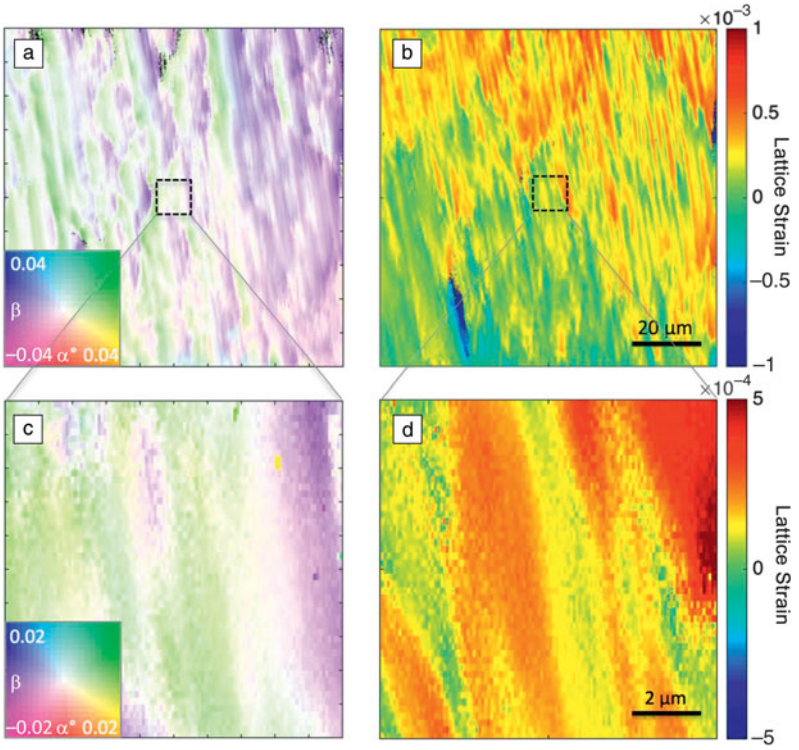


Figure 6. False-color maps of (a) orientation and (b) strain in the $KNbO_3$ crystal. Zoomed in images of the (c) orientation and (d) strain from the centers of the maps show local gradients around stripe-like domains. The orientation and strain maps correspond to the same region of the sample and are shown at the same scale. The local orientation in terms of sample tilt (α, β) (as per Figure 1) in (a) and (c) corresponds to the keys in the bottom left corner of the images. The local lattice strain in (b) and (d) corresponds to the key on the right side of the images.[28]

These results have significant and far-reaching implications for ferroelectric and other ferroic materials, such as shape memory and superelastic alloys. The cumulative effects of strain and orientation gradients at domain walls imply that the local polarization at such boundaries must be significantly augmented by both direct lattice rotation and flexoelectric effects.[29] These observations constitute a significant step forward in the direct characterization of complex multiscale phenomena in these materials, and are directly comparable to similar multiscale models from, for example, phase-field techniques.[30]

Mapping dislocations

Visualizing the 3D dislocation structure within single crystals, grains, or domains is essential to understand micromechanics and is vital for controlling the performance, for example,

https://doi.org/10.1557/mrs.2016.114 Published online by Cambridge University Press

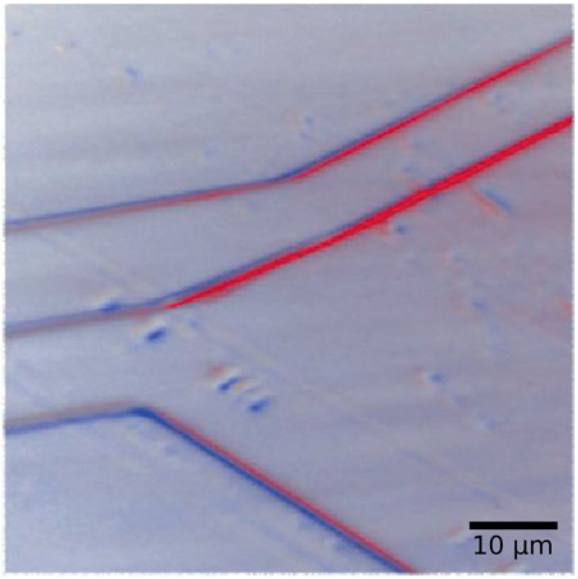


Figure 7. False-color image of three dislocations within a diamond crystal. Two images are superposed, the red and blue ones representing an offset in the axial strain of $+3 \times 10^{-4}$ and -3×10^{-4}, respectively. The sample was fully illuminated and, as such, the image is a projection.[34]

of photovoltaics and microelectronics. Traditionally, TEM is used to visualize the dislocation structure due to the high-contrast and high-resolution images obtained from the technique, even in 3D.[31] However, the small samples are subject to spurious boundary conditions from the surfaces. X-ray topography, on the other hand, can visualize hundreds of dislocations in centimeter-sized single crystals and can be generalized to 3D reconstructions.[32] However, the spatial resolution of the "direct beam" approach used is inherently limited to approximately 10 µm,[33] putting a severe upper limit on the detectible dislocation densities for which it is applicable.

The dark-field microscope provides an image of the regions in the sample that are both within the direct-space field of view and give rise to diffraction in the range of angles accepted by the objective. The angular resolution is sufficiently good in that the microscope can be set to focus on parts of the tails of the scattering, thus excluding the response from the main peak. The "weak beam" scattering defined in this way will be approximately kinematical in nature. Furthermore, by acquiring images as a function of distance to the main peak in reciprocal space, one can map strain components in 3D. This is illustrated in **Figure 7** for the case of a diamond crystal.[34] As expected, upon crossing a dislocation line, the strain is inverted, as seen by the change from red to blue color in Figure 7. The sharpness of the dislocation topology in the high-strain regions near the core implies that the detectable dislocation density is dictated by the spatial resolution of the microscope. These results point to a route for experimentally addressing dislocation dynamics.

We emphasize that only three of the nine components of the displacement gradient tensor can be measured from the type of mapping previously described, as we only probe one diffraction vector, **Q**. To map all components, it is required to repeat the data acquisition for at least two additional reflections. (Likewise, to map full orientations and not just pole figures, two reflections are required.) To facilitate this, the microscope at the ID06 beamline can operate with the objective and far-field detector both in the horizontal and vertical planes.

Outlook

Dark-field x-ray microscopy is a promising technique for comprehensive multiscale studies of self-organization, domain evolution, transport, and the role of defects within crystalline materials. In addition, we can highlight two further potential applications:

- *In operando* studies of devices–Spatially localized phenomena govern the performance and lifetime of many devices or components. Dark-field x-ray microscopy would enable one to directly record movies of the structural changes taking place at embedded interfaces in, for example, electrochemical cells or microelectromechanical devices.
- Nucleation–Nucleation processes (e.g., phases, grains, and domains) determine transformation rates, yet mechanisms are often not known, and quantitative data for simulation models is sparse. With this technique, we can map sufficiently large specimens to identify such events, and zoom in on individual nuclei to retrieve crucial local parameters, such as wetting angles and orientation relationships.

Like electron microscopes, this approach can easily incorporate additional modalities, such as bright-field microscopy,[35] high-resolution x-ray microscopy,[36] and small-angle x-ray scattering microscopy,[37] as well as the use of coherent x-ray nanobeams for ultimate resolutions.[38–40]

With continual improvements in hard x-ray optics, such as multilayer Laue lenses, improved spatial resolution is also expected in the coming years.[41] While temporal resolution (and thus the suitability for *in situ* measurements of structural dynamics) is presently limited by the photon flux of the x-ray source, upcoming "ultimate storage rings"[42] in fourth-generation synchrotrons promise to improve this by several orders of magnitude.

References

1. H.H. Liu, S. Schmidt, H.F. Poulsen, A. Godfrey, Z.Q. Liu, J. Sharon, X. Huang, *Science* **332**, 833 (2011).
2. P.A. Midgley, R.E. Dunin-Borkowski, *Nat. Mater.* **8**, 271 (2009).
3. N. Zaafarani, D. Raabe, R.N. Singh, F. Roters, S. Zaefferer, *Acta Mater.* **54**, 1863 (2006).
4. M.D. Uchic, M.A. Groeber, D.M. Dimiduk, J.P. Simmons, *Scr. Mater.* **55**, 23 (2006).
5. B.C. Larson, W. Yang, G.E. Ice, J.D. Budai, J.Z. Tischler, *Nature* **415**, 887 (2002).
6. F. Hofmann, B. Abbey, W. Liu, R. Xu, B.F. Usher, E. Balaur, Y. Liu, *Nat. Commun.* **4**, 2774 (2014).
7. C.G. Schroer, O. Kurapova, J. Patommel, P. Boye, J. Feldkamp, B. Lengeler, M. Burghammer, C. Riekel, L. Vince, A. van der Hart, M. Küchler, *Appl. Phys. Lett.* **87**, 124103 (2005).

https://doi.org/10.1557/mrs.2016.114 Published online by Cambridge University Press

8. H. Mimura, S. Handa, T. Kimura, H. Yumoto, D. Yamakawa, H. Yokoyama, S. Matsuyama, K. Inagaki, K. Yamamura, Y. Sano, K. Tamakaku, Y. Nishino, M. Yabashi, T. Ishikawa, K. Yamauchi, *Nat. Phys.* **6**, 122 (2010).
9. G. Ice, J.D. Budai, J.W.L. Pang, *Science* **334**, 1234 (2011).
10. M. Dierolf, A. Menzel, P. Thibault, P. Schneider, C.M. Kewish, R. Wepf, O. Bunk, F. Pfeiffer, *Nature* **467**, 436 (2010).
11. M.A. Pfeifer, G.J. Williams, I.A. Vartanyants, R. Harder, I.K. Robinson, *Nature* **442**, 63 (2006).
12. D. Shapiro, P. Thibault, T. Beetz, V. Elser, M. Howells, C. Jacobsen, J. Kirz, E. Lima, H. Miao, A. Neiman, D. Sayre, *Proc. Natl. Acad. Sci. U.S.A.* **102**, 15343 (2005).
13. H.F. Poulsen, S.F. Nielsen, E.M. Lauridsen, S. Schmidt, R.M. Suter, U. Lienert, L. Margulies, T. Lorentzen, D.J. Jensen, *J. Appl. Crystallogr.* **34**, 751 (2001).
14. S. Schmidt, S.F. Nielsen, C. Gundlach, L. Margulies, X. Huang, D.J. Jensen, *Science* **305**, 229 (2004).
15. B. Jakobsen, H.F. Poulsen, U. Lienert, J. Almer, S.D. Shastri, H.O. Sørensen, C. Gundlach, W. Pantleon, *Science* **312**, 889 (2006).
16. C.M. Hefferan, J. Lind, S.F. Li, U. Lienert, A.D. Rollett, R.M. Suter, *Acta Mater.* **60**, 4311 (2012).
17. A. King, G. Johnson, D. Engelberg, W. Ludwig, J. Marrow, *Science* **321**, 382 (2008).
18. W. Ludwig, P. Reischig, A. King, M. Herbig, E.M. Lauridsen, G. Johnson, T.J. Marrow, J.-Y. Buffière. *Rev. Sci. Instrum.* **80**, 033905 (2009).
19. F. Stöhr, J. Wright, H. Simons, J. Michael-Lindhard, J. Hübner, F. Jensen, O. Hansen, H.F. Poulsen. *J. Micromech. Microeng.* **25**, 125013 (2015).
20. W. Ludwig, P. Cloetens, J. Härtwig, J. Baruchel, B. Hamelin, P. Bastie, *J. Appl. Crystallogr.* **34**, 602 (2001).
21. A. Snigirev, V. Kohn, I. Snigireva, B. Lengeler, *Nature* **384**, 49 (1996).
22. H. Simons, A. King, W. Ludwig, C. Detlefs, W. Pantleon, S. Schmidt, F. Stöhr, I. Snigireva, A. Snigirev, H.F. Poulsen. *Nat. Commun.* **6**, 6098 (2015).
23. S.R. Ahl, H. Simons, A.C. Jakobsen, Y.B. Zhang, F. Stöhr. D. Juul Jensen, H.F. Poulsen, *IOP Conf. Ser. Mater. Sci. Eng.* **89**, 012016 (2015).
24. S.R. Ahl, H. Simons, A.C. Jakobsen, D.J. Jensen, H.F. Poulsen, "Multiscale 3D Mapping of Embedded Recrystallizing Grains in Aluminum," Oral presentation at the 3rd International Congress on 3D Materials Science (3DMS), St. Charles, IL, July 10–13 2016 (accepted), http://www.tms.org/Meetings/2016/3DMS2016/technicalProgram.aspx#.Vye5A5N95E4.
25. D. Damjanovic, *Rep. Prog. Phys.* **61**, 1267 (1998).
26. J. Siedel, L.W. Martin, Q. He, Q. Zhan, Y.-H. Chu, A. Rother, M.E. Hawkridge, P. Maksymovych, P. Yu, M. Gajek, N. Balke, S.V. Kalinen, S. Gemming, F. Wang, G. Catalan, J.F. Scott, N.A. Spaldin, J. Orenstein, R. Ramesh, *Nat. Mater.* **8**, 229 (2009).
27. G. Catalan, A. Lubk, H.G. Vlooswijk, E. Snoeck, C. Magen, A. Janssens, G. Rispens, G. Rijnders, D.H.A. Blank, B. Noheda, *Nat. Mater.* **10**, 963 (2011).
28. H. Simons, A.C. Jakobsen, S.R. Ahl, C. Detlefs, H.F. Poulsen, "Multiscale 3D Characterization with Dark-Field X-Ray Microscopy," Presented at the Danscatt Annual Meeting, Aarhus, Denmark, May 28–29 2015, http://www.bioxray.au.dk/~thirup/Danscatt2015/Programme.pdf.
29. P. Zubko, G. Catalan, A.K. Tagantsev, *Annu. Rev. Mater. Res.* **43**, 387 (2013).
30. Y. Gu, M. Li, A.N. Morozovska, Y. Wang, E.A. Eliseev, V. Gopolan, L.-Q. Chen, *Phys. Rev. B Condens. Matter* **89**, 174111 (2014).
31. G.S. Liu, S.D. House, J. Kacher, M. Tanaka, K. Higashida, I.M. Robertson, *Mater. Charact.* **87**, 1 (2014).
32. D. Hänscke, L. Helfen, V. Altapova, A. Danilewsky, T. Baumbach, *Appl. Phys. Lett.* **101**, 244103 (2012).
33. B.K. Tanner, *X-ray Diffraction Topography* (Pergamon Press, Oxford, UK, 1976).
34. A.C. Jakobsen, H. Simons, S.R. Ahl, C. Detlefs, J. Härtwig, H.F. Poulsen, "Mapping of Embedded Dislocations in Diamond with Sub 200 nm Resolution," Oral presentation at the 3rd International Congress on 3D Materials Science (3DMS), St. Charles, IL, July 10–13 2016 (accepted), http://www.tms.org/Meetings/2016/3DMS2016/technicalProgram.aspx#.Vye5A5N95E4.
35. R.H. Mathiesen, L. Arnberg, Y. Li, V. Meier, P.L. Schaffer, I. Snigireva, A. Snigirev, A.K. Dahle, *Metall. Mater. Trans. A* **42**, 170 (2010).
36. A. Bosak, I. Snigireva, K.S. Napolskii, A. Snigirev, *Adv. Mater.* **22**, 3256 (2010).
37. M.M. van Schooneveld, J. Hilhorst, A.V. Petukhov, T. Tyliszczak, J.A. Wang, B.M. Weckhuysen, F.M.F. de Groot, E. de Smit, *Small* **7**, 804 (2011).
38. I. Robinson, R. Harder, *Nat. Mater.* **8**, 291 (2009).
39. P. Thibault, M. Dierolf, A. Menzel, O. Bunk, C. David, F. Pfeiffer, *Science* **321**, 379 (2008).
40. P. Godard, G. Carbone, M. Allain, F. Mastropietro, G. Chen, L. Capello, A. Diaz, T.H. Metzger, J. Stangl, V. Chamard, *Nat. Commun.* **2**, 568 (2011).
41. A.J. Morgan, M. Prasciolu, A. Andrejczuk, J. Krzywinski, A. Meents, D. Pennicard, H. Graafsma, A. Barty, R.J. Bean, M. Barthelmess, D. Oberthuer, O. Yefanov, A. Aquila, H.N. Chapman, S. Bajt, *Sci. Rep.* **5**, 9892 (2015).
42. M. Eriksson, J. van der Veen, C. Quitmann, *J. Synchrotron Radiat.* **21**, 837 (2014). □



https://doi.org/10.1557/mrs.2016.114 Published online by Cambridge University Press